TMX1 determines cancer cell metabolism as a thiol-based modulator of ER–mitochondria Ca^{2+} flux

Arun Raturi,[1]* Tomás Gutiérrez,[1]* Carolina Ortiz-Sandoval,[1] Araya Ruangkittisakul,[2] Maria Sol Herrera-Cruz,[1] Jeremy P. Rockley,[1] Kevin Gesson,[1] Dimitar Ourdev,[1] Phing-How Lou,[3] Eliana Lucchinetti,[3] Nasser Tahbaz,[1] Michael Zaugg,[3] Shairaz Baksh,[4,5,6,7] Klaus Ballanyi,[2] and Thomas Simmen[1]

[1]Department of Cell Biology, [2]Department of Physiology, [3]Department of Anesthesiology and Pain Medicine, [4]Department of Pediatrics, [5]Department of Biochemistry, and [6]Department of Oncology, Faculty of Medicine and Dentistry, University of Alberta, Edmonton, Alberta T6G2H7, Canada
[7]Alberta Inflammatory Bowel Disease Consortium, University of Alberta, Edmonton, Alberta T6G2H7, Canada

The flux of Ca^{2+} from the endoplasmic reticulum (ER) to mitochondria regulates mitochondria metabolism. Within tumor tissue, mitochondria metabolism is frequently repressed, leading to chemotherapy resistance and increased growth of the tumor mass. Therefore, altered ER–mitochondria Ca^{2+} flux could be a cancer hallmark, but only a few regulatory proteins of this mechanism are currently known. One candidate is the redox-sensitive oxidoreductase TMX1 that is enriched on the mitochondria-associated membrane (MAM), the site of ER–mitochondria Ca^{2+} flux. Our findings demonstrate that cancer cells with low TMX1 exhibit increased ER Ca^{2+}, accelerated cytosolic Ca^{2+} clearance, and reduced Ca^{2+} transfer to mitochondria. Thus, low levels of TMX1 reduce ER–mitochondria contacts, shift bioenergetics away from mitochondria, and accelerate tumor growth. For its role in intracellular ER–mitochondria Ca^{2+} flux, TMX1 requires its thioredoxin motif and palmitoylation to target to the MAM. As a thiol-based tumor suppressor, TMX1 increases mitochondrial ATP production and apoptosis progression.

Introduction

Ca^{2+} flux from the endoplasmic reticulum (ER) to mitochondria has emerged as an important regulator of mitochondrial oxidative phosphorylation (Cárdenas et al., 2010) and apoptosis progression (Boehning et al., 2004, 2005). This ion flux is caused by Ca^{2+} release from the ER through various Ca^{2+} channels (Raturi et al., 2014). Subsequently, Ca^{2+} either reenters the ER through the sarco-ER Ca^{2+} transport ATPase (SERCA; Waldeck-Weiermair et al., 2013) or transfers over to mitochondria via the mitochondrial Ca^{2+} uniporter (MCU; Patron et al., 2013). This bidirectional Ca^{2+} flux between the ER and mitochondria occurs at the mitochondria-associated membrane (MAM; Vance, 1990; Rizzuto et al., 1998; Csordás and Hajnóczky, 2009). Here, Ca^{2+} handling proteins tune their activity to match the amount of unfolded proteins within the ER. Upon ER stress, the interaction between the ER and mitochondria increases, which results in an increased MAM-associated Ca^{2+} flux and enhanced ATP production (Csordás et al., 2006; Bravo et al., 2011).

The connection between ER protein folding and mitochondrial Ca^{2+} influx is highlighted by regulatory, redox-sensitive interactions of ER chaperones and oxidoreductases with Ca^{2+} handling proteins (Simmen et al., 2010). Two examples are ERp44, which interacts with inositol 1,4,5-triphosphate receptor type 1 (IP_3R1), and calnexin, which interacts with SERCA2b (Higo et al., 2005; Lynes et al., 2013). Through this function, ER chaperones and other redox-sensitive proteins may play an important role for normal mitochondrial metabolism (Csordás et al., 2006; Bravo et al., 2011). Consistent with this, the activity of calnexin on SERCA2b results in a reduction of ER–mitochondrial Ca^{2+} cross talk that determines mitochondrial bioenergetics (Cárdenas et al., 2010), as shown by two very different approaches (Roderick et al., 2000; Lynes et al., 2013).

In this study, we aimed to gain further insight into how MAM-localized folding enzymes influence ER–mitochondria Ca^{2+} flux. We focused on the ER-localized thioredoxin-related transmembrane protein 1 (TMX1) that targets to the MAM in a palmitoylation-dependent manner (Roth et al., 2009; Lynes et al., 2012). This protein disulfide isomerase (PDI)–related protein can retain misfolded major histocompatability complex

*A. Raturi and T. Gutiérrez contributed equally to this paper.

Correspondence to Thomas Simmen: thomas.simmen@ualberta.ca

A. Raturi's present address is Dept. of Oncology, University of Alberta, Edmonton, Alberta T6G2H7, Canada.

K. Gesson's present address is Max F. Perutz Laboratories, 1030 Vienna, Austria.

Abbreviations used: AMPK, adenosine monophosphate–activated protein kinase; BAPTA-AM, 1,2-bis(*o*-aminophenoxy)ethane-*N*,*N*,*N*′,*N*′-tetraacetic acid; KD, knockdown; KO, knockout; LAR-ER-GECO, low-affinity ER R-GECO; MAM, mitochondria-associated membrane; MCU, mitochondrial Ca^{2+} uniporter; MEF, mouse embryonic fibroblast; NAC, *N*-acetyl cysteine; R-GECO, red fluorescent genetically encoded Ca^{2+} indicator for optical imaging; ROS, reactive oxygen species; SERCA, sarco-ER Ca^{2+} transport ATPase; WT, wild type.

The Rockefeller University Press $30.00
J. Cell Biol. Vol. 214 No. 4 433–444
www.jcb.org/cgi/doi/10.1083/jcb.201512077

class I variants (Matsuo et al., 2009) and preferentially interacts with transmembrane ER substrates (Pisoni et al., 2015). Both findings are consistent with the observation that most of TMX1 is found in its reduced form within the ER (Matsuo et al., 2009; Roth et al., 2009).

Our results expand the repertoire of functions for TMX1 by demonstrating that it interacts with SERCA2b under oxidizing conditions in a thiol-dependent manner to decrease SERCA activity and, thus, the ER Ca^{2+} load. Conversely, low levels of TMX1 achieved via knockout (KO) and knockdown (KD) lead to increased retention of Ca^{2+} within the ER and, hence, reduced ability of the ER to direct Ca^{2+} toward mitochondria. The reduced Ca^{2+} flux associated with low levels of TMX1 exacerbates the block of mitochondria activity in tumor cells (Warburg effect), a determinant of the growth of tumors (Ward and Thompson, 2012).

Results

TMX1 binds to SERCA2b in a calnexin-dependent manner

Our finding that TMX1 is a MAM-localized oxidoreductase (Lynes et al., 2012) suggested that it could perform a role in the regulation of ER–mitochondria Ca^{2+} flux. To test this hypothesis, we first examined the ability of TMX1 to interact with ER Ca^{2+} handling proteins. Although we were unable to detect stable interaction with IP_3Rs (not depicted), we could detect interaction between TMX1 and SERCA2b when immunoprecipitating myc-tagged SERCA2b from A375P melanoma and HeLa cell lysates and probing for endogenous TMX1 (Fig. 1 A and not depicted). Next, given TMX1 can interact with calnexin (Pisoni et al., 2015), we aimed to determine whether TMX1 and calnexin could cross-influence their interactions with SERCA2b. To test this, we first expressed FLAG-tagged TMX1 in HeLa cells, leading to approximately twice as much TMX1 (Fig. 3 A) and again immunoprecipitated myc-tagged SERCA2b. Under these conditions, we were unable to detect a change in the amount of calnexin that associated with the Ca^{2+} pump (Fig. 1 B). Next, we cotransfected wild-type (WT) mouse embryonic fibroblasts (MEFs) or calnexin KO MEFs with myc-tagged SERCA2b and FLAG-tagged TMX1. This experiment demonstrated that calnexin KO cells showed more robust interaction of the oxidoreductase with SERCA2b (Fig. 1 C). We next decided to generate TMX1 KD cell lines in WT HeLa and A375P melanoma cells (Fig. 1 D). We complemented our investigation on the function of TMX1 using the CRISPR/Cas9 KO strategy, which led to heterozygous TMX1 KO clones (subsequently called TMX1 KO) in HeLa, which exhibited undetectable levels of TMX1 (Fig. 1 D). Interestingly, TMX1 KO cells showed more calnexin coimmunoprecipitating with SERCA2b than control HeLa cells (Fig. 1 E). Together, our results showed that although TMX1 was not able to reduce calnexin binding to SERCA2b below a threshold level, the absence of either TMX1 or calnexin boosted interaction with SERCA2b for the other.

Loss of TMX1 activates SERCA-mediated Ca^{2+} import into the ER

Our findings so far indicated that TMX1 could modulate SERCA activity similar to calnexin to control ER Ca^{2+} homeostasis. We tested this hypothesis by quantifying the ability of the ER to take up Ca^{2+} with an aequorin-based approach (Alvarez and Montero, 2002). This demonstrated that both TMX1 KD and KO clones generated in HeLa or A375P cells were able to import 30–70% more Ca^{2+} into the ER (Fig. 1 F and Fig. S1 A). We repeated this experiment under more physiological conditions with ER-targeted low-affinity genetically encoded Ca^{2+} indicators for optical imaging (Wu et al., 2014). When Ca^{2+}-depleted HeLa WT and TMX1 KO cells were incubated in Ca^{2+}-containing medium, KO cells were able to take up >50% more Ca^{2+} than WT HeLa cells (Fig. 1 G). Likewise, when shifting the cells to Ca^{2+}-free medium containing the SERCA inhibitor 2,5-di(tert-butyl)-1, 4-benzo-hydroquinone (tert-BuBHQ), TMX1 KO cells exhibited an over 50% larger drop of the ER-localized, Ca^{2+}-connected fluorescence when compared with WT HeLa cells (Fig. 1 H).

Together, our results indicated that expression of TMX1 inhibits SERCA activity. Consistent with this, the reduction of TMX1 protein levels results in increased Ca^{2+} content inside the ER, which is opposite to the lower Ca^{2+} entry into the ER in MEFs lacking calnexin (Lynes et al., 2013), a known controller of ER–mitochondria Ca^{2+} flux.

Low expression of TMX1 impairs ER–mitochondria Ca^{2+} flux

To further test the phenotype and consequences of low TMX1 expression, we analyzed how the observed increased ER Ca^{2+} retention impacted global Ca^{2+} homeostasis. To do so, we again used control HeLa and TMX1 KO cells and opened up their IP_3Rs using histamine. As previously observed by others (De Marchi et al., 2011), we surmised that improved Ca^{2+} uptake and higher ER Ca^{2+} content in TMX1 KO cells should manifest in lower relative Ca^{2+} drop, as measured via ER-targeted low-affinity genetically encoded Ca^{2+} indicators for optical imaging. Indeed, the proportional drop in fluorescence signal in TMX1 KO cells was only ∼60% of the one found in WT HeLa cells (Fig. 2 A). We next investigated the consequences of this phenotype for cytosolic Ca^{2+} availability and clearance in WT HeLa or TMX1 KO or KD HeLa cells. In the presence of extracellular Ca^{2+}, this was reflected by a minor reduction of the FURA-2 peak by 20% in TMX1 KO and 30% in TMX1 KD HeLa cells, when compared with control (Fig. 2 B). Next, we incubated WT and TMX1 KO HeLa cells in Ca^{2+}-free medium and released an aliquot of the remaining Ca^{2+} through IP_3Rs. Although we did not detect significantly different amounts of Ca^{2+} released by TMX1 KO cells into the cytosol, they cleared this Ca^{2+} faster than WT HeLa cells (Fig. 2 C), except when coincubated with the irreversible SERCA-inhibitor thapsigargin (Fig. S1 B), indeed confirming that TMX1 influences the ER Ca^{2+} content by activating SERCA.

Next, we analyzed Ca^{2+} transfer from the ER to mitochondria using mitochondrially targeted red fluorescent genetically encoded Ca^{2+} indicator for optical imaging (R-GECO; Wu et al., 2014). Consistent with the increased retention of ER Ca^{2+} (Fig. 2, A and C), we detected a roughly 50% decrease in the relative availability of Ca^{2+} within mitochondria upon histamine-mediated Ca^{2+} release in TMX1 KO and KD cells (Fig. 2, D and E), regardless of the presence of Ca^{2+} in the culture medium. Given the importance of Ca^{2+} transfer from the ER to mitochondria for ER–mitochondria apposition (Csordás et al., 2010; Qi et al., 2015), we next investigated whether contacts between the two organelles were altered upon TMX1 KO. Indeed, we found that the average length of tight ER–mitochondria contacts (<50 nm) decreased from 172 nm to 127 nm (a reduction of over 25%, Fig. 2 F). To-

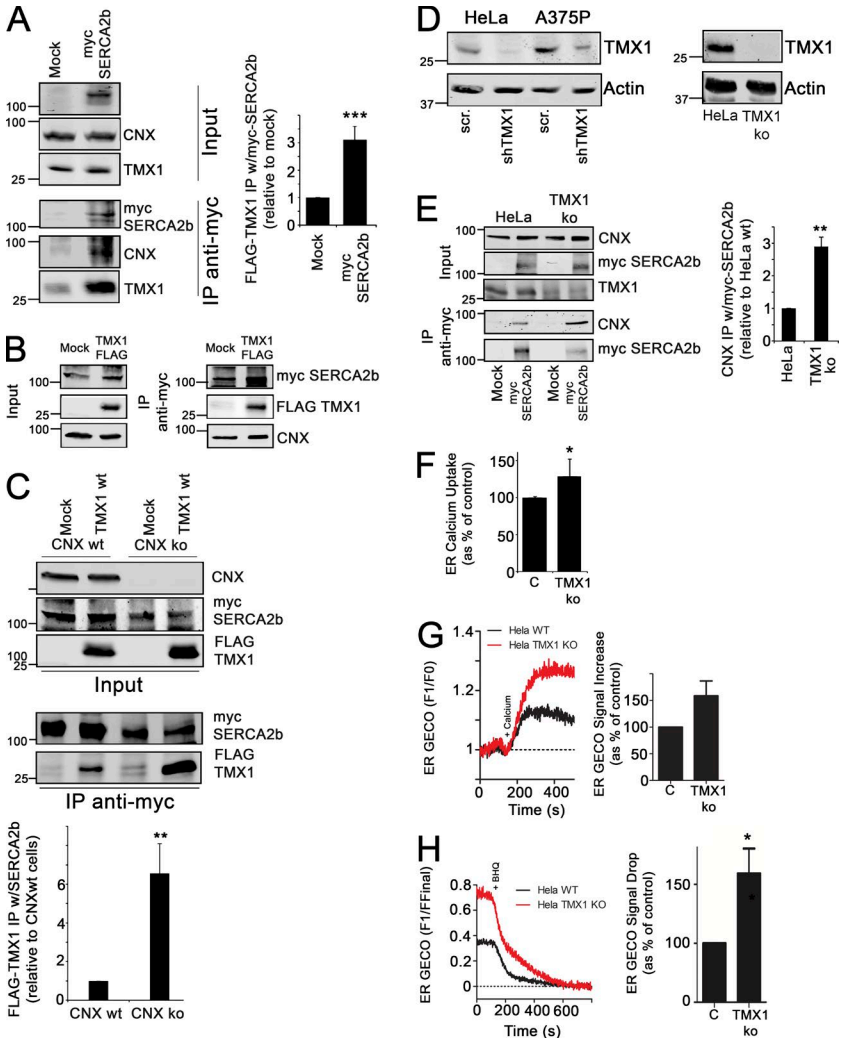

Figure 1. **TMX1 thioredoxin and palmitoylation motifs regulate interaction with SERCA2b.** (A) TMX1-SERCA2b coimmunoprecipitation. A375P cells were transfected with mycSERCA2b. DSP cross-linked lysates (5% inputs, left) and myc immunoprecipitates (IP) were analyzed for calnexin (CNX) and coimmunoprecipitating endogenous TMX1. The signal of TMX1 immunoprecipitated together with mycSERCA2b was expressed relative to the background. *n* = 3; ***, P = 0.001 (standard error expressed vs. Mock). (B) TMX1 does not disrupt calnexin–SERCA2b interaction. Control and TMX1-transfected HeLa cells were transfected with mycSERCA2b. DSP-cross-linked lysates (5% inputs, left) and myc immunoprecipitates were analyzed for calnexin and coimmunoprecipitating endogenous TMX1. (C) TMX1-SERCA2b interaction depends on calnexin. Calnexin WT and KO MEFs were transfected with mycSERCA2b and FLAG-tagged TMX1 as indicated. DSP cross-linked lysates (5% inputs, left) and myc immunoprecipitates were analyzed for coimmunoprecipitating FLAG-tagged TMX1. *n* = 4; **, P = 0.0114 for immunoprecipitation (standard error expressed vs. wild type). (D) Analysis of TMX1 heterozygous KO and shTMX1-transfected HeLa and A375P lysates. TMX1 heterozygous KO HeLa cells were generated with the CRISPR/Cas9 method. Their lysates and control lysates were probed with our anti-TMX1 antibody. For KD, HeLa and A375P cells were stably transfected with shTMX1 and probed with an anti-TMX1 antibody. (E) Calnexin-SERCA2b interaction depends on TMX1. TMX1 WT and KO HeLa cells were transfected with mycSERCA2b. DSP cross-linked lysates (5% inputs, left) and myc immunoprecipitates were analyzed for coimmunoprecipitating calnexin. *n* = 3; **, P = 0.005 (standard error expressed vs. HeLa). (F) Measurement of global ER Ca^{2+} uptake. HeLa heterozygous KO cells were cotransfected with a plasmid encoding ER-targeted aequorin. Luminescence was plotted from three independent experiments. *, P = 0.02 (standard error expressed vs. HeLa). (G) ER Ca^{2+} uptake in intact cells. HeLa heterozygous KO cells were cotransfected with a plasmid encoding LAR-ER-GECO. Ca^{2+} was depleted with reversible tert-BuBHQ and Ca^{2+} was added back at 1 mM in tert-BuBHQ–free medium. Relative fluorescence increase was plotted and quantified from four independent experiments (P = 0.06; standard error expressed vs. HeLa). (H) ER Ca^{2+} leak in intact cells. HeLa heterozygous KO cells were cotransfected with a plasmid encoding LAR-ER-GECO. Ca^{2+} was depleted with reversible tert-BuBHQ. Relative fluorescence decrease was plotted and quantified from seven independent experiments (*, P = 0.03; standard error expressed vs. HeLa).

gether, our results demonstrate that cells with low expression of TMX1 retain Ca^{2+} better within the ER and transfer less Ca^{2+} less to mitochondria, concomitant with reduced ER–mitochondria apposition.

MAM-localized TMX1 is a thiol-dependent modulator of ER–mitochondria Ca^{2+} flux

Next, we tested whether the TMX1-SERCA2b interaction is localization and thiol dependent and if so, whether the manipulation of these two properties of TMX1 could impact on Ca^{2+} flux. Our experiments also aimed to answer whether TMX1 overexpression increases ER–mitochondria Ca^{2+} flux, opposite to TMX1 KD or KO. To use mutant TMX1, we transfected TMX1 KO cells with WT TMX1 and its mutants or naturally low-expressing A375P cells (Lynes et al., 2012), which led to a doubling of the amounts of TMX1 in A375P when compared with control cells (Fig. 3 A).

As a first test for redox sensitivity of the TMX1–SERCA2b pair, we examined whether cellular oxidation by buthionine sulfoximine, known to increase ER–mitochondria Ca^{2+} flux (Hawkins et al., 2010; Redpath et al., 2013), leads to increased interaction between SERCA2b and TMX1. Indeed, buthionine sulfoximine promoted the interaction, whereas glutathione ester that increases cellular reduction of glutathione decreased it (Fig. S1 C). In addition, oxidation resulted in a relative shift of TMX1 toward the MAM portion of the ER, whereas glutathione ester reversed this shift (Fig. S1 D). We next decided to mutagenize the redox-responsive, highly conserved thioredoxin motif of TMX1 and altered the two cysteines of the CXXC active site to serines (SXXS mutant). We tested TMX1 and this mutant for their oxidoreductase activity by incubating wild type and mutant TMX1 with dieosin glutathione disulfide, which fluoresces 70-fold more upon reduction of its disulfide bond (Raturi and

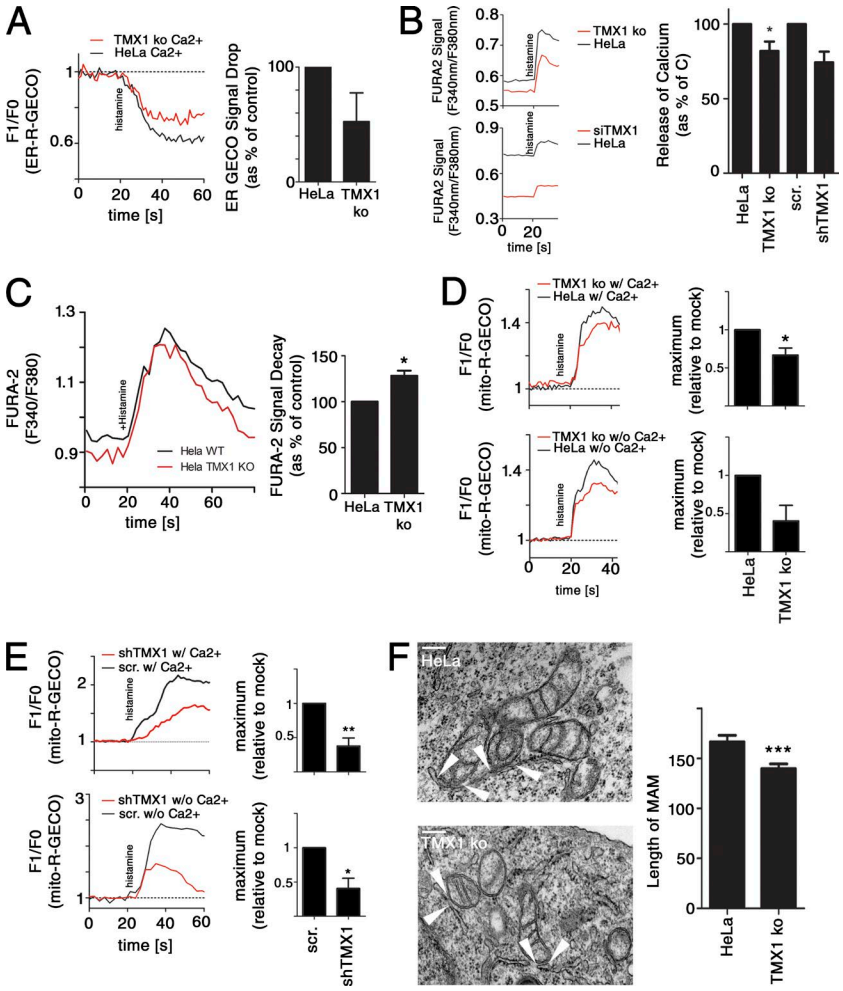

Figure 2. **Decreased expression of TMX1 inhibits ER-derived Ca^{2+} flux.** (A) Measurement of ER Ca^{2+} content change after histamine-mediated ER calcium release. HeLa control and heterozygous KO cells were transfected with LAR-ER-GECO. Ca^{2+} was released with histamine, and probe fluorescence was recorded before and after 50 µM histamine treatment by fluorescence microscopy. Relative fluorescence decrease was plotted and quantified from three independent experiments (P = 0.017; standard error expressed vs. HeLa). (B) Measurement of cytosolic Ca^{2+} concentration after histamine-mediated ER Ca^{2+} release. Representative FURA-2-derived curves from TMX1 heterozygous KO and KD cells are plotted and quantified from five independent experiments; standard error expressed versus HeLa or scrambled control (*, P = 0.02 for WT vs. KO). (C) Measurement of cytosolic Ca^{2+} clearance after histamine-mediated ER calcium release. HeLa control and heterozygous KO cells were loaded with FURA-2. Ca^{2+} was released with histamine and probe fluorescence was recorded before and after 50 µM histamine treatment on a fluorimeter. Data were derived from four independent experiments (*, P = 0.014; standard error expressed vs. HeLa). (D) Measurement of mitochondrial Ca^{2+} after histamine-mediated ER Ca^{2+} release. HeLa and TMX1 heterozygous KO HeLa cells were transfected with mitochondrial R-GECO1 and treated with 50 µM histamine, followed by probe fluorescence recording. Results are summarized as a graph representing maximum response. Data were derived from six independent experiments for with Ca^{2+} (*, P = 0.01) and from three independent experiments for without Ca^{2+}; standard error expressed versus HeLa. (E) Measurement of mitochondrial Ca^{2+} after histamine-mediated ER Ca^{2+} release. HeLa and A375P cells transfected with shTMX1 plasmids and mitochondrial R-GECO1 were treated with 50 µM histamine, and probe fluorescence was recorded. Results from three independent experiments each are summarized as a graph representing maximum response. **, P = 0.001 for with Ca^{2+}; *, P = 0.05 for without Ca^{2+}. (F) Electron micrograph analysis of control and TMX1 heterozygous KO HeLa cells. One representative electron micrograph, respectively, is shown. Analysis and quantification of the distance of 595 MAMs for WT and 648 MAMs for KO is shown as a bar graph; standard error indicated (***, P = 0.0001). Bars, 150 nm.

Mutus, 2007). We indeed detected reductase activity for wild type TMX1 (Fig. 3 B), consistent with previous studies (Matsuo et al., 2004), but not with the TMX1 SXXS mutant, as expected.

To address the role of TMX1 localization, we used a mutant where two cytosolic cysteines have been changed to alanines (CCAA), which abolishes palmitoylation and MAM enrichment of TMX1 (Figs. 3 C and S1 E). With TMX1 mutants compromised for MAM localization and reductase activity in hand, we were able to determine that both are required for the interaction of TMX1 with SERCA2b (Figs. 3 D and S1 F).

We next measured whether increasing TMX1 expression decreases ER Ca^{2+} uptake. We found that the overexpression of WT TMX1 led to an over 50% reduction of ER Ca^{2+} that was not observed to the same extent with thioredoxin-mutated TMX1 SXXS. Conversely, the TMX1 mutant most defective in MAM enrichment (CCAA; Fig. 3 E) exhibited an intermediate phenotype. We also tested whether the overexpression of ER-restricted TMX1 and its mutants improved mitochondrial Ca^{2+} uptake. Indeed, this was the case, as higher levels of TMX1, but not of its mutants increased relative histamine-controlled Ca^{2+} transfer to mitochondria, as measured using mitochondrially targeted R-GECO (Fig. 3, F and G), as well as Rhod2 (Fig. S2 A). Therefore, our overexpression studies confirmed that TMX1 increased ER–mitochondria Ca^{2+} flux in a thiol- and localization-dependent manner.

TMX1 determines mitochondria metabolism from the ER

Our findings so far had identified TMX1 as a regulator of ER–mitochondria Ca^{2+} flux and ER–mitochondria apposition, and we next aimed to determine whether it also impacts mitochondrial bioenergetics. We first determined the respiratory capacity of HeLa (Fig. 4, A and B) and A375P cells (Fig. 4 C), where we had manipulated TMX1 expression levels. Our results showed that the mitochondrial capacity of HeLa cells with low TMX1 expression was reduced by almost 50% (Fig. 4, A and B). Conversely, we observed a 20% increase in mitochondrial capacity in A375P cells, where we had achieved the doubling of TMX1 expression (Fig. 4 C) and, in contrast, a reduction of oxygen consumption by 30% in A375P cells transfected with TMX1 siRNA, respectively. To examine how these changes impacted cellular bioenergetics, we measured the cellular ATP content.

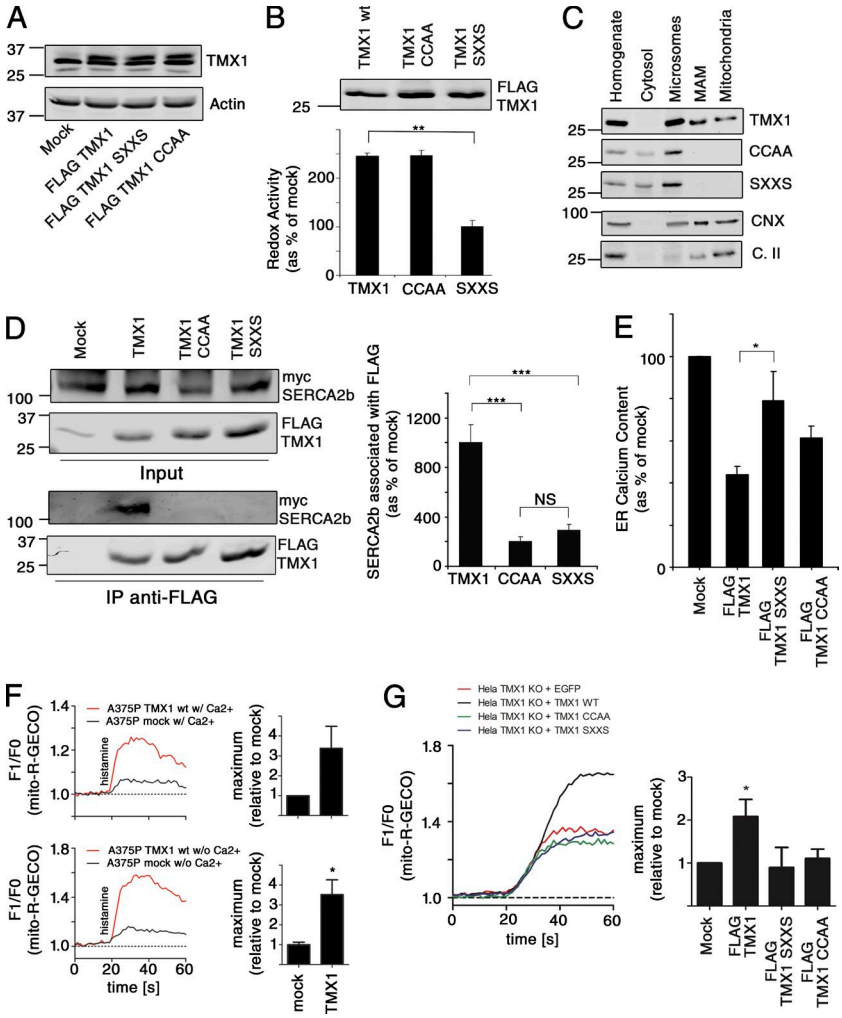

Figure 3. **Increased expression of TMX1 inhibits ER Ca^{2+} uptake but promotes ER-derived Ca^{2+} flux.** (A) Analysis of TMX1-transfected A375P lysates. A375P cells were stably transfected with TMX1 constructs as indicated and probed with our anti-TMX1 antibody. (B) TMX1 redox activity. TMX1 disulfide reduction activity was measured by adding immunoprecipitated TMX1 or its mutants (TMX-SXXS or TMX-CCAA) to 100 nM Di-E-GSSG in the presence of 5 µM DTT. The graph plots the increase in fluorescence versus nontransfected control immunoprecipitate. The gel on top shows lysates from a typical experiment analyzed for the FLAG-TMX1 content via Western blot. **, P < 0.01; standard error indicated. (C) TMX1 and TMX1 mutant distribution among microsomes (containing ER, endosomes, and lysosomes), mitochondria, and the MAM. HeLa homogenates from cells transfected with pcDNA3 or plasmids expressing FLAG-tagged WT TMX1 or the CCAA or SXXS mutants were fractionated via the Percoll fractionation protocol into cytosol, microsomes, pure mitochondria, and MAM, as indicated on the right side. Equal cell equivalents have been loaded, and TMX1 was detected via its FLAG tag. (D) TMX1-SERCA2b interaction depends on TMX1 redox activity and localization. A375P cells were transfected with mycSERCA2b and FLAG-tagged TMX1 mutants as indicated. DSP cross-linked lysates (5% inputs, left) and myc immunoprecipitates were analyzed for coimmunoprecipitating FLAG-tagged TMX1. *n* = 3; ***, P = 0.000197 for TMX WT versus SXXS. ***, P = 0.000013 and 0.000011 for immunoprecipitation; standard error indicated. (E) Measurement of ER Ca^{2+} content. A375P cells were transfected with TMX1 constructs as indicated and cotransfected with a plasmid encoding ER-targeted aequorin. Luminescence was plotted from three independent experiments. *, P = 0.01; standard error expressed versus A375P. (F) Measurement of mitochondrial Ca^{2+} after histamine-triggered Ca^{2+} release. A375P cells transfected with TMX1 and mitochondrial R-GECO1 were treated with 50 µM histamine, and probe fluorescence was recorded. Results from three independent experiments are summarized as a graph representing maximum response. Experiments were done in the presence and absence of extracellular Ca^{2+}. Differences are not statistically significant with Ca^{2+} but significant without Ca^{2+} (*, P = 0.01; standard error expressed vs. A375P). (G) Measurement of mitochondrial Ca^{2+} after histamine-triggered Ca^{2+} release in heterozygous TMX1 KO HeLa cells rescued with TMX1 or its mutants. TMX1 KO HeLa cells rescued with TMX1 or its mutants (identified via fluorescence signal derived from pIRES-EGFP) were transfected with mitochondrial R-GECO1 and treated with 50 µM histamine in the absence of extracellular Ca^{2+}, and probe fluorescence was recorded. Results from three independent experiments are summarized as a graph representing maximum response and slope of the signal increase (*, P = 0.03 for FLAG-TMX1; standard error expressed vs. HeLa).

Consistent with our results on mitochondrial oxygen consumption, we detected a reduction of the cellular ATP content in TMX1 HeLa KO and KD cells by >25% (Figs. 4 D and S2 B). We also detected a reduction of the cellular ATP content by 30–40% in HeLa and A375P cells stably transfected with TMX1 RNAi but almost 20% higher ATP levels in cells stably transfected with WT TMX1 cDNA (Fig. S2 B). To test whether this change in ATP production was indeed tied to a loss of redox-sensitive ER–mitochondria Ca^{2+} flux in TMX1 KO cells, we treated control and KO cells with the Ca^{2+} chelator 1,2-bis(*o*-aminophenoxy)ethane-*N*,*N*,*N*′,*N*′-tetraacetic acid (BAPTA-AM) and the antioxidant *N*-acetyl cysteine (NAC). We found evidence for our hypothesis by showing that reduced ATP levels reached in TMX1 KO cells could not be significantly further reduced by either BAPTA-AM or NAC treatment (Fig. 4 F).

We next assayed for potential changes in the mitochondrial proteome that could cause the changes that we had observed with altered TMX1 expression levels. However, we were unable to detect changes in the mitochondrial proteome, including enzymes catalyzing mitochondrial oxidative phosphorylation (mitochondrial complex II and mitochondrial cytochrome *c*) or peroxisome proliferator–activated receptor c coactivator 1 α (PGC-1α; Austin and St-Pierre, 2012), that could explain our findings via other mechanisms (Fig. S2 C) or the MCU (not depicted; Filadi et al., 2015). In contrast, we were able to detect significant increases in the phosphorylation of 5′ adenosine monophosphate–activated protein kinase (AMPK; Fig. 4 G). Therefore, low levels of TMX1 reduce mitochondrial respiration and ATP levels that subsequently activate the AMPK signaling machinery, whereas increased levels of TMX1 show the opposite phenotype.

We next asked how cells with low TMX1 survive, given that cell lines such as HeLa normally exhibit robust mitochondrial energy production (Reitzer et al., 1979; Jouaville et al., 1999; Favre et al., 2010). To answer this question, we glucose-starved transfectants with low or high levels of TMX1 generated in HeLa (Fig. 5, A and B) or A375P cells (Fig. 5 C). This condition demonstrated that cells with low levels of TMX1 are dependent on the presence of glucose. Whereas TMX1 KO cells show a slightly elevated level of cell death, this increases almost threefold in the

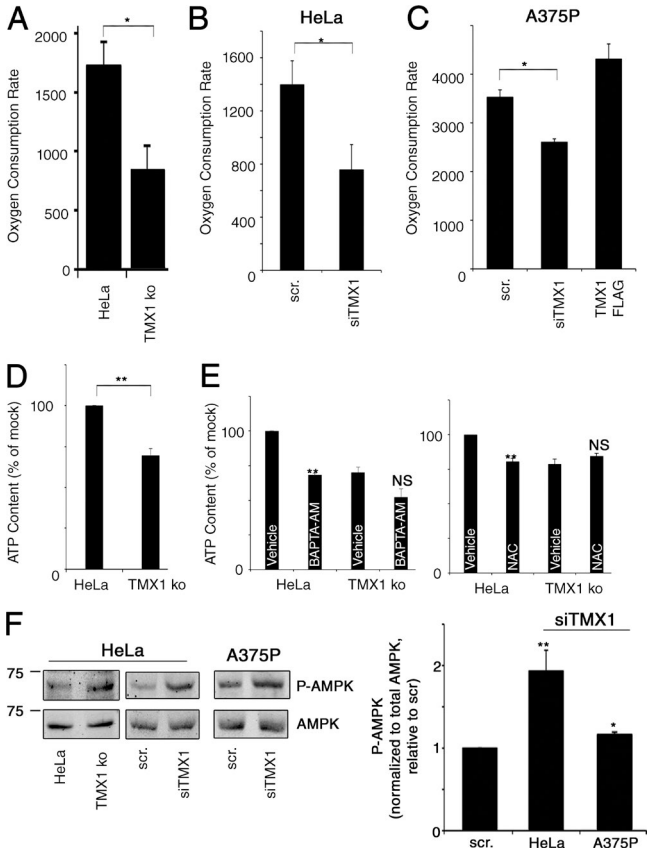

Figure 4. **TMX1 regulates mitochondrial energy production.** (A) Measurement of the mitochondrial oxygen consumption rate, expressed as the maximal respiration ETC capacity (picomoles of O_2 per second per citrate synthase (CS) activity, see Materials and methods) in control HeLa cells and TMX1 heterozygous KO HeLa cells. Results from three independent experiments are summarized as a graph (*, P = 0.026; standard error indicated). (B) Measurement of the mitochondrial oxygen consumption rate (picomoles O_2 per second per CS activity, see Materials and methods) in control HeLa cells and cells transfected with siTMX1. Results from three independent experiments are summarized as a graph (*, P = 0.014; standard error indicated). (C) Measurement of the mitochondrial oxygen consumption rate (picomoles O_2 per second per CS activity) in control A375P cells and cells transfected with FLAG-tagged TMX1 or siTMX1. Results from three independent experiments are summarized as a graph (*, P = 0.018; standard error indicated). (D) Measurement of cellular ATP content (see Materials and methods) in control HeLa and heterozygous TMX1 KO HeLa cells. Results from three independent experiments are summarized as a graph (n = 9; **, P = 0.042; standard error indicated). (E) Measurement of cellular ATP content in control HeLa and heterozygous TMX1 KO HeLa cells treated with 10 µM BAPTA-AM and 10 mM NAC. Results from three experiments are summarized. **, P = 0.001 for WT BAPTA-AM, 0.05 for KO BAPTA-AM; **, P = 0.001 for WT NAC, 0.12 for KO NAC; standard error expressed versus HeLa. (F) Analysis of HeLa control and TMX1 KO and A375P lysates transiently transfected as indicated with RNAi against TMX1. Lysates were probed for phospho-AMPK and normalized to total AMPK. Representative gels are shown. The graph plots the levels of phosphorylated AMPK in cells transfected with TMX1 RNAi versus control cells transfected with scrambled RNAi (n = 3; **, P = 0.003 for HeLa; *, P = 0.02 for A375P; standard error expressed vs. scrambled controls).

absence of glucose for 24 h (Fig. 5 A). After 48 h, transfection of TMX1 siRNA led to even more marked reductions of survival in these culture conditions, whereas its overexpression had the reverse effect (Fig. 5, B and C). Interestingly, the low expression of TMX1 also increased reactive oxygen species (ROS; Fig. 5 D), especially in TMX1 KO cells, but did not result in ER stress (Fig. S2 D). We were also unable to detect any changes in the autophagy markers p62 or LC3-II levels (Fig. S2 E). Consistent with the increased presence of dying cells (Fig. 5 A) and their increased levels of ROS (Fig. 5 D), TMX1 KO and KD cells showed reduced growth that resulted in a roughly 100% increase of their doubling times (Figs. 5 E and S2 F). Finally, we tested whether TMX1 KD potentially promotes aerobic glycolysis, as suggested by their decreased oxygen consumption (Fig. 4, A–C), and their glucose addiction (Fig. 5, A–C). Therefore, we analyzed cellular lysates of HeLa and A375P cells with altered TMX1 expression for the presence of hexokinases I and II, the latter being a marker for tumor cells that exhibit high levels of aerobic glycolysis (Pastorino and Hoek, 2003). Although our cell lines had increased levels of hexokinase II when TMX1 was low (Fig. 5 F), the removal of glucose did not reproducibly reduce cellular ATP content any further than what we observed in TMX1 WT cells (not depicted). Collectively, our results demonstrate that TMX1 controls cellular metabolism and in particular mitochondrial bioenergetics. The reduction of TMX1 expression results in cell lines becoming increasingly glucose addicted and characterized by high levels of ROS.

TMX1 determines tumor growth in vivo

Our previous results led to the hypothesis that TMX1 could influence tumor growth via its role in mitochondria metabolism. We tested this hypothesis from three angles: first, by examining whether tumor tissue has lower TMX1 levels than healthy tissue; second, by further analyzing growth properties of TMX1 shRNA clones; and third, by mouse xenograft assays.

As an exploratory experiment, we homogenized tissue obtained from metastatic melanoma patients. When comparing the protein amounts of TMX1, we noticed that TMX1 expression was lower compared with normal skin (Fig. S2 G). For the remaining experiments, we used shTMX1, rather than TMX1 KO HeLa cells, because the latter showed ongoing cell death (Fig. 5 A). Our previous results indicated that low TMX1 leads to glucose addiction, suggesting that their mitochondria might be less critical for survival. Indeed, shTMX1 HeLa cells showed less susceptibility to the mitochondrial poisons rotenone and antimycin (Fig. 6 A). Because low mitochondrial activity contributes to growth medium acidification, we found that shTMX1 indeed also leads to this effect (Fig. 6 B).

Next, we injected the HeLa and A375P cell lines subcutaneously into nude mice. This set-up led to the visible appearance of tumor masses in <50 d with HeLa cells stably expressing TMX1 shRNA, compared with 85 d with control HeLa cells (Fig. 6 C). In the case of A375P cells, after tumor growth for 35 d, we detected an almost twofold growth increase for A375P cells stably expressing TMX1 shRNA, but less than half for A375P cells overexpressing TMX1 (Fig. 6 D).

Therefore, consistent with our in vitro results, we demonstrate that TMX1 can also control tumor growth properties in vivo. The reduction of TMX1 expression increases the speed of tumor growth, whereas higher levels of TMX1 expression lead to a slowdown.

Discussion

Our previous work had demonstrated that the ER-restricted, palmitoylated PDI family protein TMX1 localizes to the MAM (Lynes et al., 2012). This localization suggests that despite the presence of a thioredoxin domain, the primary function of

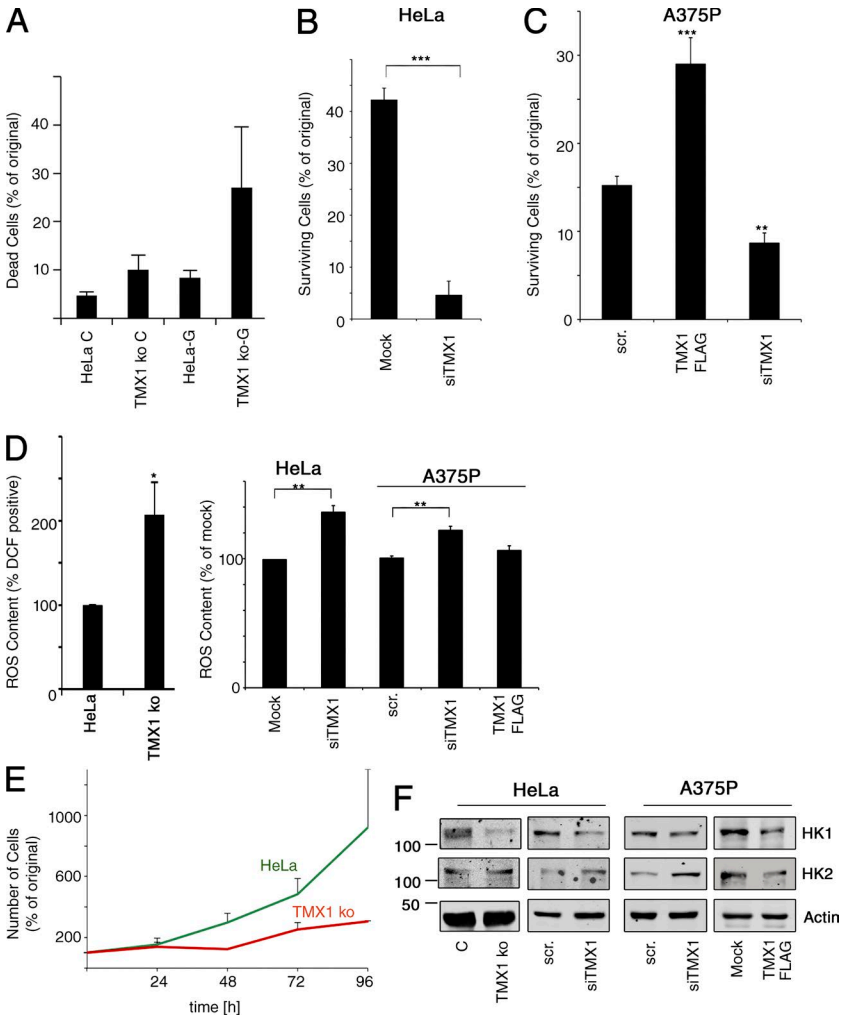

Figure 5. **Altered mitochondria metabolism increases ROS and glucose dependence in cells expressing low amounts of TMX1.** (A) Quantification of surviving cells upon 24-h glucose deprivation. HeLa cells and TMX1 heterozygous KO HeLa cells were incubated in glucose-free medium (supplemented with galactose) or control condtions (C) and subsequently analyzed for positive Annexin V and propidium iodide (PI) signals. The amount of dead cells was normalized to controls, and results from three independent experiments were graphed. P > 0.05 for all; standard error indicated. (B) Quantification of surviving HeLa cells upon glucose deprivation. Cells were transfected with RNAi against TMX1. After 48 h, cells were incubated in glucose-free medium (supplemented with galactose) and subsequently analyzed for positive Annexin V and PI signals. The amount of dead cells was normalized to the scrambled siRNA controls, and results from three independent experiments were graphed. ***, P < 0.000001; standard error indicated. (C) Quantification of surviving A375P cells upon glucose deprivation. Cells were transfected with RNAi against TMX1, as well as a plasmid encoding for FLAG-tagged TMX1. After 48 h, cells were incubated in glucose-free medium (supplemented with galactose) and subsequently analyzed for positive Annexin V and PI signals. The amount of dead cells was normalized to the scrambled siRNA controls, and results from three independent experiments were graphed. ***, P = 0.001679 for FLAG-TMX1; **, P = 0.01947 for siTMX1; standard error indicated. (D) Measurement of the cellular ROS production via DCF in control HeLa and TMX1 heterozygous KO cells (left). ROS-dependent fluorescence was determined via flow cytometry. Results from three independent experiments are summarized as a graph (*, P = 0.01; standard error expressed vs. HeLa). Measurement of the cellular ROS production via HyPer in control HeLa and A375P cells and cells transfected with FLAG-tagged TMX1 as well as siTMX1 (right). ROS-dependent fluorescence was determined via flow cytometry. Results from three independent experiments are summarized as a graph (**, P = 0.00038 for HeLa and 0.0027 for A375P; standard error expressed vs. HeLa and A375P controls). (E) Growth curve for HeLa WT and heterozygous TMX1 KO cells. Cells were seeded at 100,000 per well, and cells were quantified 24, 48, 72, and 96 h after seeding; standard error indicated. (F) Assessment of glycolytic enzymes. Analysis of HeLa control and TMX1 heterozygous KO and A375P lysates transfected as indicated with FLAG-tagged TMX1 or siTMX1. Lysates were probed for hexokinases I and II and normalized to actin.

TMX1 may lie elsewhere than in protein folding, which occurs on the rER (Lynes and Simmen, 2011). Indeed, our results show that TMX1 is a regulator of cellular Ca^{2+} flux. TMX1 normally augments Ca^{2+} release at the MAM, which can then migrate to mitochondria to stimulate oxidative phosphorylation. To do so, TMX1 interacts with SERCA2b in a redox-dependent manner (Fig. 1, A and B). Accordingly, we showed that the ER Ca^{2+} content of cells overexpressing TMX1 was 50% lower than control cells. No such effect could be detected for TMX1, where we had mutated the CXXC active site to SXXS (Fig. 3 E). Conversely, the nonpalmitoylated TMX1 CCAA mutant showed partial activity.

We observed the opposite effect when we reduced TMX1 expression: these cells had 30–70% higher Ca^{2+} content within the ER (Fig. 1, F and G; and Fig. S1 A). This led to increased Ca^{2+} loss from the ER upon SERCA inhibition, and faster cytosolic Ca^{2+} clearance (Figs. 1 H and 2 C). Our results are consistent with TMX1 acting as an inhibitor of SERCA2b, reducing the import of cytosolic Ca^{2+} into the ER. Importantly, when interfering with TMX1 via mutagenesis, KO or reduction of its expression, the effects are not limited to the ER. Instead, its activity fans out and determines Ca^{2+} flux to mitochondria (Figs. 2 and 3). This flux is now recognized as a determinant of mitochondrial bioenergetics (Cárdenas et al., 2010). Therefore, when we interfered with TMX1, we observed multiple changes in mitochondria metabolism, including oxygen consumption rate (Fig. 4, A–C) and ATP production (Fig. 4 D). These changes were Ca^{2+} flux and redox dependent (Fig. 4, D and F), consistent with our model, where TMX1 acts as a thiol- and palmitoylation-dependent modulator of cytosolic Ca^{2+} availability for mitochondria.

One area that requires further attention is how TMX1 executes this modulatory activity on SERCA2b. One possibility is that TMX1 acts as a reductase on the luminal cysteine bond of SERCA2b (Appenzeller-Herzog and Simmen, 2016), but it is

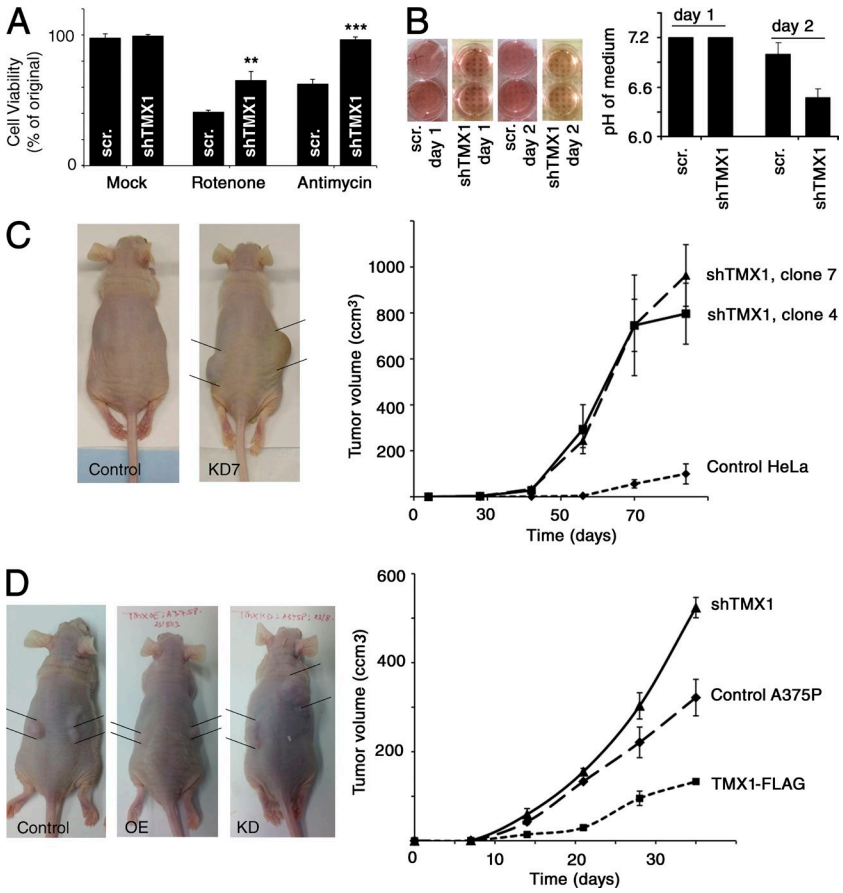

Figure 6. **Low TMX1 expression accelerates tumor growth in vivo.** (A) Quantification of surviving cells upon interference with mitochondria metabolism. HeLa cells and TMX1 heterozygous KO HeLa cells were incubated in medium supplemented with rotenone or antimycin and subsequently analyzed for positive Annexin V and propidium iodide signals. The amount of dead cells was normalized to the scrambled siRNA controls, and results from three independent experiments were graphed. $n = 3$; **, $P = 0.02$ for rotenone. $n = 3$; ***, $P = 0.00$ for antimycin. Standard error expressed versus scrambled Mock control. (B) Determination of medium acidification. HeLa cells and TMX1 heterozygous KO HeLa cells were plated into 24-well dishes, and the pH of the medium was determined after 24 and 48 h of culture ($n = 3$). Standard error expressed versus scrambled day 1. (C) Tumor growth of TMX1 HeLa KD clones in vivo. HeLa clones stably transfected with pcDNA3 or TMX1 shRNA (clones 4 and 7) were injected subcutaneously into the right and left flanks of athymic nude mice. The images show representative euthanized mice with their tumors marked on the side, and the graph summarizes the results of three animals each; standard error indicated. (D) Tumor growth of TMX1 A375P KD and overexpression (OE) clones in vivo. A375P clones stably transfected with pcDNA3, FLAG-tagged TMX1, or TMX1 shRNA were injected subcutaneously into the right and left flanks of athymic nude mice. The images show representative euthanized mice with their tumors marked on the side, and the graph summarizes the results of three animals each; standard error indicated.

probably less likely to interact in the cytosol, where oxidation of cysteines determines SERCA activity in a bell-shaped manner (Adachi et al., 2004).

The changes in cellular metabolism observed upon interference with TMX1 raise the interesting question of how the cell copes with them. One critical observation in cells with reduced levels of TMX1 is a reduction of ER–mitochondria contacts (Fig. 2 F), known to occur in tumor tissues for over 60 yr (Howatson and Ham, 1955). Interestingly, the TMX1 KD phenotype is strikingly similar to cells with low mitofusin-2 expression, which also have increased SERCA activity accompanied with compromised MAM (de Brito and Scorrano, 2008) and increased xenograft growth (Rehman et al., 2012).

Another way that cancer cells with low levels of TMX1 could compensate is by increasing their glycolytic phenotype, but that does not occur in this case (Fig. 4 F), potentially explaining why low levels of TMX1 result in increased amounts of ROS (Fig. 5 D), a mild increase in constitutive cell death in KO cells (Fig. 5 A), and decreased growth under laboratory culture conditions (Fig. 5 E). This latter observation is, however, not unusual for a tumor-promoting mutation or deletion, as shown by the example of Bak/Bax double KO cells (Jones et al., 2007), which are interestingly also defective for ER Ca^{2+} mobilization. Moreover, we were unable to create a homozygous KO in HeLa and A375P tumor cell lines, consistent with the recently identified dependence of tumor cells on ER–mitochondria Ca^{2+} flux (Cárdenas et al., 2016). Our results suggest that low TMX1 expression enhances the Warburg phenotype (Warburg, 1956), consistent with a resistance of TMX1-depleted cells to mitochondrial poisons (Fig. 6 A) and their ability to acidify the growth medium (Fig. 6 B).

This important insight prompted us to investigate a potential tumor-suppressing role of TMX1, as also supported by the observation of reduced levels of TMX1 upon breast cancer progression and upon asbestos exposure of lung cells (Nymark et al., 2007; Lagadec et al., 2012). In short, our results have identified a novel, thiol-dependent mechanism based on tumor suppressing TMX1.

Materials and methods

Antibodies and reagents

All chemicals were obtained from Sigma-Aldrich, except OptiPrep (Axis-Shield), DCF (Thermo Fisher Scientific), and Percoll (GE Healthcare). Antibodies were purchased from Sigma-Aldrich against TMX1 and LC3 (rabbit antihuman); from EMD Millipore against SERCA2b (mouse antihuman) and against total as well as phosphorylated AMPK (rabbit antihuman); from Thermo Fisher Scientific against PDI, CHOP, and actin (mouse antihuman); from BD against BiP/GRP78 and p62 (mouse antihuman); from Abcam against FACL4 (goat antihuman), mitochondrial complex II (mouse antihuman), and PGC-1α (rabbit antihuman); and from Cell Signaling Technology. The antibodies against anti-myc (Invitrogen) and the FLAG tag (Rockland) were purchased as indicated. We thank L. Berthiaume (University of Alberta, Alberta, Canada) for the goat anti–human cytochrome *c*. The affinity-purified rabbit anti-TMX1 antiserum was generated by 21st Century Biochemicals using a peptide corresponding to amino acids 251–271 (AESKEGTNKDFPQNAIRQRSL). The rabbit anti–calnexin antibody has been previously described (Myhill et al., 2008). HeLa cells were from ECACC, and A375P cells were from E. Sviderskaya

(St. George's, University of London, London, England, UK). Melanoma tissue samples were purchased from the Alberta Tumor Bank.

Expression vectors, RNAi, and mutagenesis

FLAG-tagged TMX1 was generated by PCR using oligos TS470, TS244, TS363, TS364 and TS368 (Fig. S3 A) on a human IMAGE TMX1 EST clone (Invitrogen) by inserting the FLAG-coding sequences to generate a signal peptide cleavage site after glycine 20. The full-length product was cloned into pcDNA3 and pIRES2-EGFP (Takara Bio Inc.) plasmids using the 5′ Kpn1 or the 5′ Nhe1 site, respectively, and the 3′ Xho1 sites. Mutant TMX1 constructs were generated by PCR-based splicing by overlap extension using oligos TS369, TS370 (CCAA) and TS435, TS436 (SXXS). In brief, primary PCR products generated using TMX1 5′ (TS470) and 3′ oligos (TS368) with the mutagenizing upstream and downstream oligos were isolated. Subsequently, a secondary PCR yielded the full-length, mutated cDNA using just the 5′ and 3′ TMX1 oligos. This product was cloned into pIRES-EGFP using the Nhe1–Xho1 sites. The shTMX1 GFP construct (HSH-019885.4-CH1 in psi-H1, target sequence 5′-TCGTGCCAA GCAATAAGAT-3′) was purchased from Genecopoiea. Stealth RNAi HSS129875 (sequence 5′-TGCACAACCTTTGAAAAAAGT-3′) as well as control Stealth RNAi (Medium GC content control siRNA 12935–300) for transient expression were purchased from Invitrogen. The myc-tagged SERCA2b expression plasmid was obtained from U. Petäjä-Repo (University of Oulu, Oulu, Finland).

TMX1 CRISPR/Cas9 KO

TMX1 gene KO was performed with the KN206187 plasmid (OriGene), closely following the manufacturer's instructions. In brief, HeLa cells were transfected and passaged nine times before applying the puromycin antibiotic. After isolation of colonies on 15-cm dishes, clones were subcloned on 96-well dishes. Quantitative PCR determined the KO as heterozygous. KO was verified for the duration of the experiments by Western blot and flow cytometry for the EGFP signal. Further validation was performed by isolating genomic DNA with the QIAamp DNA Mini kit (QIAGEN), followed by PCR amplification of KO construct DNA that showed insertion of an EGFP sequence into the genomic TMX1 DNA (Fig. S3 B).

Lysate immunoblotting analysis

For the analysis of cellular proteomes, cells were plated in 150 mm culture dishes and lysed using lysis buffer (50 mM Tris-HCl, pH 7.4, 1% NP-40, 0.25% sodium deoxycholate, 150 mM Tris-HCl, 1 mM EDTA, 1 mM PMSF, 1 µg/ml leupeptin, aprotinin, and pepstatin, 1 mM NaF, and 1 mM Na_4VO_3). Lysates were centrifuged at 800 *g* for 10 min at 4°C, and supernatants were subsequently analyzed by Western blotting with the antibodies indicated, after loading equalization with actin or tubulin, as indicated.

Coimmunoprecipitation experiments

Cells were washed twice with PBS++ and incubated for 30 min at room temperature with or without 2 mM Dithiobis (succinimidyl proprionate; Thermo Fisher Scientific) in PBS++, as indicated. This cross-linker will not maintain connections in the presence of reducing sample buffer. The cells were then washed twice more and incubated in 10 mM NH4Cl in PBS++ for 10 min to quench the cross-linking reaction. The cells were then washed a final time in PBS++ and harvested in CHAPS lysis buffer (1% CHAPS, 10 mM Tris, pH 7.4, 150 mM NaCl, and 1 mM EDTA) containing Complete protease inhibitors (Roche). Postnuclear supernatants were obtained by centrifuging the lysates for 5 min at 4°C at 800 *g* and were subsequently incubated with the indicated antibodies for 1 h at 4°C on a rocker. Protein A Sepharose beads were then added and the lysates incubated for a further hour. The beads were then washed three times in CHAPS buffer, resuspended in Laemmli buffer, and analyzed by SDS-PAGE and Western blot.

OptiPrep gradient fractionation

Postnuclear membranes of HeLa and A375P cells were fractionated via OptiPrep as follows: Cells were washed twice in PBS++ and collected in mitochondria homogenization buffer (10 mM Hepes, pH 7.4, 250 mM sucrose, 1 mM EDTA, and 1 mM EGTA). The cell suspension was passed 15 times through an 18-µM clearance ball bearing homogenizer (Isobiotech). The cells were subsequently centrifuged for 10 min at 800 *g* at 4°C to pellet nuclei and unbroken cells. The supernatant was layered over a 10–30% continuous gradient of OptiPrep density gradient medium (Axis-Shield) and centrifuged in an SW55 Ti rotor (Beckman Coulter) for 3 h at 32,700 rpm. Six fractions were taken from the top of the gradient and analyzed by SDS-PAGE and Western blot.

Monitoring TMX1 reductase activity

DiEGSSG was prepared as described before (Raturi and Mutus, 2007). In brief, 100 µM GSSG was incubated with 10-fold molar excess of 1 mM eosin isothiocyanate in phosphate buffer (100 mM potassium phosphate and 2 mM EDTA, pH 8.8) at RT (25°C) and purified using G-25 columns (100 × 10 mm) in phosphate buffer, pH 7.4. TMX1 disulfide reduction activity was measured by adding immunoprecipitated TMX1 or its mutants (TMX-SXXS or TMXCCAA) to 100 nM DiEGSSG in the presence of 5 µM DTT. The increase in fluorescence was monitored at 545 nm with excitation at 525 nm using an 814 photomultiplier detection system (PTI).

Measurement of calcium content and flux

ER Ca^{2+} uptake was measured with pHSVerAEQ (a gift from J. Alvarez, Universidad de Valladoid, Valladolid, Spain). WT, KD, and KO cells were transfected with this plasmid (and constructs expressing TMX1, as indicated) and processed for measurements 24 h after transfection as described previously (Alvarez and Montero, 2002). In brief, ER Ca^{2+} was depleted in buffer 1 (145 mM NaCl, 5 mM KCl, 1 mM MgCl, 10 mM glucose, and 10 mM Hepes, pH 7.4) containing 0.5 mM EGTA and 60 µM of the reversible SERCA inhibitor 2,5-di-tert-butylbenzohydroquinone (Sigma-Aldrich) for 15 min at 37°C. Subsequently, aequorin was reconstituted in the dark by incubating in buffer 1 containing 5 µM coelenterazine hcp (Sigma-Aldrich) for another 30 min. Uptake was determined as the rise of luminescence on a Lumat luminometer (Berthold) from before to after Ca^{2+} perfusion with 1 mM $CaCl_2$ in buffer 1, expressed relative to control cells. Maximum response was elicited subsequently by adding 0.1% Triton X-100 to check that luminescence had not been depleted during the experiment.

To measure ER Ca^{2+} release into the cytosol, we used Fura-2. 10^6 cells (as indicated in the experiments) were seeded in 35-mm plates. The next day, cells were washed with HBSS buffer (Thermo Fisher Scientific) containing 140 mg/l Ca^{2+}, 100 mg/l Mg^{2+} and 0.1% BSA (HBSS/Ca/Mg/BSA) and then incubated with 1 ml 1 µM Fura-2 in HBSS/Ca/Mg/BSA for 30 min at RT in the dark. Next, we replaced the loading medium with HBSS/Ca/Mg/BSA and incubated for a further 15 min in the dark. After trypsinization and quenching with 1 ml DMEM/10% FBS, cells were washed twice with 1 ml HBSS/Ca/Mg/BSA. Cells were then resuspended in HBSS/Ca/Mg/BSA and transferred into a cuvette containing a stirring bar, followed by the measuring of 505 nm emission with 340/380 nm excitation on an 814 photomultiplier detection system (PTI), upon establishment of a 200-s baseline. Drugs (50 µM histamine or 10 µM thapsigargin) were added as 100 µl of a 200× stock solution prepared in HBSS/Ca/Mg/BSA. The Ca^{2+} response was determined as the relative ratiometric signal

obtained from the baseline and after adding drugs. For the decay calculation, we fit a line into the data derived from the peak until 30 s later. Data were analyzed using the LibreOffice Spreadsheet software.

To measure ER and mitochondrial Ca^{2+}, 50,000 cells were grown for 1 d in 35-mm glass-bottom dishes (MatTek Corporation) and transfected with 0.5 µg of the Ca^{2+} indicator plasmids low-affinity ER R-GECO (LAR-ER-GECO) or mitochondrial R-GECO (Wu et al., 2014) using 2.5 µg Metafectene (Biontex) and following the manufacturer's protocol. On the day of the experiment, the perfusion system was equilibrated with the appropriate HBSS solution (HBSS/Ca/Mg or HBSS−; 0.1 mM EGTA, 1.75 mM $MgCl_2$, and 0.41 mM $MgSO_4$), as indicated. 30 s after the start of the experiment, the medium was changed to the stimulus as indicated for a duration of 5–10 min, followed by continuing the run of the experiment for 10 min using HBSS/Ca/Mg or HBSS−, respectively. For these single-cell experiments, as indicated in figure legends, *n* refers to number of experiments, each consisting of multiple numbers of cells (at least 5 to typically 12).

Microscopy and image acquisition

All microscopy experiments were performed on an FV1000 laser-scanning confocal microscope (Olympus) using a 20× objective (XLUMPL ANFL, NA 1.0; Olympus), equipped with perfusion systems using a peristaltic pump (for the FV1000 system, Watson-Marlow Alitea-AB; Sin-Can). Live-cell images were taken every second with a 559 nm laser excitation and a 575–675 nm band-pass emission filter using a PL-A686 6.6 megapixel camera (Capture-se software; PixeLINK). Temperature in the recording chamber was kept at 25–27°C (TC-324B; Harvard Apparatus). Cells were incubated in tissue culture medium supplemented with drugs as indicated. Fluorochromes were used as indicated. Acquisition occurred with the Olympus Fluoview software, and image quantification was performed with the Fiji distribution of ImageJ.

ATP content

Cellular ATP content was determined using the ATP Determination kit (Molecular Probes; emission ∼560 nm at pH 7.8) as per the manufacturer's instruction manual (Thermo Fisher Scientific). Readings were normalized to the number of viable cells using trypan blue exclusion method.

Apoptosis measurements, medium acidification, and ROS content

Apoptosis of cells in glucose-free medium was assayed as follows: Cells (as indicated) were seeded at 500,000 into 6-well dishes. The next day, the normal growth medium was exchanged to DMEM containing 2 mM glutamine. 48 h later, cells were processed for Annexin V staining using the Annexin V-Cy3 Apoptosis detection kit (Biovision). In brief, cells were trypsinized and resuspended in PBS containing 1% BSA. They were then incubated with 5 µl Annexin V-Cy3 in 500 µl binding buffer (following the manufacturer's instructions) and sorted on an LSR Fortessa (BD). Medium acidification was measured as follows: 250,000 cells were plated per well in a 12-well plate. The conditioned growth medium was removed after 24 and 48 h, and the pH was measured using a Mettler pH meter. To measure cellular ROS, cells were cotransfected with HyPer plasmid for 24 h (Evrogen) or loaded for 30 min with 5 µM dichlorofluorescein, and ROS was measured by flow cytometry.

Mitochondrial oxygen consumption

The respiratory capacity of the mitochondrial electron transport chain was measured in intact cells using high-resolution respirometry (Oxygraph-2K; Oroboros) at 37°C, as previously described (Lucchinetti et al., 2012). Cultured cells were trypsinized, centrifuged at 100 *g* for 5 min, resuspended in the same media and immediately assessed for O_2 consumption in a single protocol designed to assess basal respiration; ATP turnover respiration (after addition of the ATP synthase inhibitor oligomycin), and maximal respiration (or electron transfer system capacity, after addition of the protonophoric uncoupler carbonyl cyanide-4-[trifluoromethoxy]phenylhydrazone). Data were normalized to citrate synthase activity (Srere, 1969).

In vivo tumor xenograft

WT TMX1 cDNA and shRNA clones generated in A375P or HeLa (as indicated) were trypsinized. 10×10^6 cells were injected subcutaneously into the right and left flanks of athymic nude mice (#NCRNU-M, CrTac :NCr-FoxN1Nu; Taconic). Mice were monitored weekly until tumors appear and then twice a week thereafter. Once tumors exceeded 20 mm in diameter ((length × width^2)/2), mice were euthanized and tumors excised and measured. All animal experiments were conducted as per the guidelines of the University of Alberta Animal Policy and Welfare Committee and the Canadian Council on Animal Care Guidelines. The approval for use of animals in research was granted by the Animal Care and Use Committee for Health Sciences, a University of Alberta ethics review committee.

Preparation and analysis of electron micrographs

Cell monolayers were fixed for 20 min using 2% paraformaldehyde and 2% glutharaldehyde in 100 mM sodium cocadylate buffer, pH 7.4. Cells were scraped from the plates and pelleted. Secondary fixation was in osmium tetroxide 1% followed by quick rinses in water and staining in 1% aqueous solution of uranyl acetate. Dehydration was in increasing concentrations of ethanol followed by incubation in propylene oxide at RT. Pellets were then infused with Embed 812, and blocks were hardened at 60°C for a minimum of 48 h. We used an Ultracut E (Reichert-Jung) for sectioning and imaged the samples using a CCD camera (iTEM; Olympus Soft Imaging Solutions) mounted on a 410 transmission electron microscope (Philips). On the images, we identified ER tubules in the proximity of mitochondria and determined their distance in nanometers. We recorded apposed ER tubules per mitochondrion (distance <50 nm) and quantified their distance and length for control and KO conditions. Average distance was 20 µm, and no significant differences in length were seen for contacts >30 nm in distance. Data were derived from over 100 images for HeLa WT and KO cells each, covering $n = 595$ MAMs for WT and $n = 648$ MAMs for KO.

Statistical analysis

Unless specified otherwise, all the data are expressed as mean ± standard deviation from a minimum of three determinations. Bar graphs include standard errors. Statistical significance of differences between various samples was determined by analysis of variance. $P < 0.05$ was considered significant. Statistical analysis was performed using the LibreOffice Calc software.

Online supplemental material

Fig. S1 provides characterization of ER Ca^{2+} uptake in RNAi clones and TMX1 behavior upon redox modulation, as well as coimmunoprecipitation of TMX1 mutants without cross-linker and their fractionation on an OPTIPREP gradient. Fig. S2 provides Rhod2 data from TMX1 mutant-transfected A375P cells and ATP content of transiently transfected cells, as well as proteomic analysis of key proteins and a growth curve of RNAi stably transfected cells. Fig. S3 provides nucleotide and CRISPR/Cas9 genomic information. Online supplemental material is available at http://www.jcb.org/cgi/content/full/jcb.201512077/DC1.

Acknowledgments

This paper is dedicated to the memory of Dr. Yvonne Dierauer.

We thank Ing-Swie Goping, Geert Bultynck, Christian Appenzeller-Herzog, Edgar Yoboue, and Roberto Sitia for helpful discussions. We thank Gary Eitzen for the use of the fluorimeter. We thank Lars-Oliver Klotz for additional compounds and helpful discussions.

Research in the Simmen laboratory was supported by Canadian Cancer Society Research Institute grant 2010-700306 and Cancer Research Society grant 18325. A. Raturi was supported by an Alberta Innovates - Health Solutions fellowship. The Zaugg laboratory was supported by grants from the Heart and Stroke Foundation of Alberta, Northwest Territories, and Nunavut (Canada) and the Mazankowski Alberta Heart Institute. The Baksh laboratory was supported by grants from Canadian Breast Cancer Foundation, Alberta Heritage Foundation for Medical Research, and Alberta Innovates - Health Solutions and a Department of Pediatrics/The Stollery Children's Foundation Hair Massacure grant generously donated by the MacDonald family. The Ballanyi laboratory was supported by an Alberta Heritage Foundation for Medical Research/Alberta Innovates - Health Solutions Scientist award, the Canada Foundation of Innovation, and Alberta Advanced Technology and Education.

The authors declare no competing financial interests.

Submitted: 23 December 2015
Accepted: 15 July 2016

References

Adachi, T., R.M. Weisbrod, D.R. Pimentel, J. Ying, V.S. Sharov, C. Schöneich, and R.A. Cohen. 2004. S-Glutathiolation by peroxynitrite activates SERCA during arterial relaxation by nitric oxide. *Nat. Med.* 10:1200–1207. http://dx.doi.org/10.1038/nm1119

Alvarez, J., and M. Montero. 2002. Measuring [Ca^{2+}] in the endoplasmic reticulum with aequorin. *Cell Calcium.* 32:251–260. http://dx.doi.org/10.1016/S0143416002001860

Appenzeller-Herzog, C., and T. Simmen. 2016. ER-luminal thiol/selenol-mediated regulation of Ca^{2+} signalling. *Biochem. Soc. Trans.* 44:452–459. http://dx.doi.org/10.1042/BST20150233

Austin, S., and J. St-Pierre. 2012. PGC1α and mitochondrial metabolism--emerging concepts and relevance in ageing and neurodegenerative disorders. *J. Cell Sci.* 125:4963–4971. http://dx.doi.org/10.1242/jcs.113662

Boehning, D., R.L. Patterson, and S.H. Snyder. 2004. Apoptosis and calcium: new roles for cytochrome c and inositol 1,4,5-trisphosphate. *Cell Cycle.* 3:252–254. http://dx.doi.org/10.4161/cc.3.3.705

Boehning, D., D.B. van Rossum, R.L. Patterson, and S.H. Snyder. 2005. A peptide inhibitor of cytochrome c/inositol 1,4,5-trisphosphate receptor binding blocks intrinsic and extrinsic cell death pathways. *Proc. Natl. Acad. Sci. USA.* 102:1466–1471. http://dx.doi.org/10.1073/pnas.0409650102

Bravo, R., J.M. Vicencio, V. Parra, R. Troncoso, J.P. Munoz, M. Bui, C. Quiroga, A.E. Rodriguez, H.E. Verdejo, J. Ferreira, et al. 2011. Increased ER-mitochondrial coupling promotes mitochondrial respiration and bioenergetics during early phases of ER stress. *J. Cell Sci.* 124:2143–2152. http://dx.doi.org/10.1242/jcs.080762

Cárdenas, C., R.A. Miller, I. Smith, T. Bui, J. Molgó, M. Müller, H. Vais, K.H. Cheung, J. Yang, I. Parker, et al. 2010. Essential regulation of cell bioenergetics by constitutive InsP3 receptor Ca^{2+} transfer to mitochondria. *Cell.* 142:270–283. http://dx.doi.org/10.1016/j.cell.2010.06.007

Cárdenas, C., M. Müller, A. McNeal, A. Lovy, F. Jaňa, G. Bustos, F. Urra, N. Smith, J. Molgó, J.A. Diehl, et al. 2016. Selective vulnerability of cancer cells by inhibition of Ca^{2+} transfer from endoplasmic reticulum to mitochondria. *Cell Reports.* 15:219–220. http://dx.doi.org/10.1016/j.celrep.2016.03.045

Csordás, G., and G. Hajnóczky. 2009. SR/ER-mitochondrial local communication: calcium and ROS. *Biochim. Biophys. Acta.* 1787:1352–1362. http://dx.doi.org/10.1016/j.bbabio.2009.06.004

Csordás, G., C. Renken, P. Várnai, L. Walter, D. Weaver, K.F. Buttle, T. Balla, C.A. Mannella, and G. Hajnóczky. 2006. Structural and functional features and significance of the physical linkage between ER and mitochondria. *J. Cell Biol.* 174:915–921. http://dx.doi.org/10.1083/jcb.200604016

Csordás, G., P. Várnai, T. Golenár, S. Roy, G. Purkins, T.G. Schneider, T. Balla, and G. Hajnóczky. 2010. Imaging interorganelle contacts and local calcium dynamics at the ER-mitochondrial interface. *Mol. Cell.* 39:121–132. http://dx.doi.org/10.1016/j.molcel.2010.06.029

de Brito, O.M., and L. Scorrano. 2008. Mitofusin 2 tethers endoplasmic reticulum to mitochondria. *Nature.* 456:605–610. http://dx.doi.org/10.1038/nature07534

De Marchi, U., C. Castelbou, and N. Demaurex. 2011. Uncoupling protein 3 (UCP3) modulates the activity of Sarco/endoplasmic reticulum Ca^{2+}-ATPase (SERCA) by decreasing mitochondrial ATP production. *J. Biol. Chem.* 286:32533–32541. http://dx.doi.org/10.1074/jbc.M110.216044

Favre, C., A. Zhdanov, M. Leahy, D. Papkovsky, and R. O'Connor. 2010. Mitochondrial pyrimidine nucleotide carrier (PNC1) regulates mitochondrial biogenesis and the invasive phenotype of cancer cells. *Oncogene.* 29:3964–3976. http://dx.doi.org/10.1038/onc.2010.146

Filadi, R., E. Greotti, G. Turacchio, A. Luini, T. Pozzan, and P. Pizzo. 2015. Mitofusin 2 ablation increases endoplasmic reticulum-mitochondria coupling. *Proc. Natl. Acad. Sci. USA.* 112:E2174–E2181. http://dx.doi.org/10.1073/pnas.1504880112

Hawkins, B.J., K.M. Irrinki, K. Mallilankaraman, Y.C. Lien, Y. Wang, C.D. Bhanumathy, R. Subbiah, M.F. Ritchie, J. Soboloff, Y. Baba, et al. 2010. S-glutathionylation activates STIM1 and alters mitochondrial homeostasis. *J. Cell Biol.* 190:391–405. http://dx.doi.org/10.1083/jcb.201004152

Higo, T., M. Hattori, T. Nakamura, T. Natsume, T. Michikawa, and K. Mikoshiba. 2005. Subtype-specific and ER lumenal environment-dependent regulation of inositol 1,4,5-trisphosphate receptor type 1 by ERp44. *Cell.* 120:85–98. http://dx.doi.org/10.1016/j.cell.2004.11.048

Howatson, A.F., and A.W. Ham. 1955. Electron microscope study of sections of two rat liver tumors. *Cancer Res.* 15:62–69.

Jones, R.G., T. Bui, C. White, M. Madesh, C.M. Krawczyk, T. Lindsten, B.J. Hawkins, S. Kubek, K.A. Frauwirth, Y.L. Wang, et al. 2007. The proapoptotic factors Bax and Bak regulate T Cell proliferation through control of endoplasmic reticulum Ca^{2+} homeostasis. *Immunity.* 27:268–280. http://dx.doi.org/10.1016/j.immuni.2007.05.023

Jouaville, L.S., P. Pinton, C. Bastianutto, G.A. Rutter, and R. Rizzuto. 1999. Regulation of mitochondrial ATP synthesis by calcium: evidence for a long-term metabolic priming. *Proc. Natl. Acad. Sci. USA.* 96:13807–13812. http://dx.doi.org/10.1073/pnas.96.24.13807

Lagadec, C., C. Dekmezian, L. Bauché, and F. Pajonk. 2012. Oxygen levels do not determine radiation survival of breast cancer stem cells. *PLoS One.* 7:e34545. http://dx.doi.org/10.1371/journal.pone.0034545

Lucchinetti, E., A.E. Awad, M. Rahman, J. Feng, P.H. Lou, L. Zhang, L. Ionescu, H. Lemieux, B. Thébaud, and M. Zaugg. 2012. Antiproliferative effects of local anesthetics on mesenchymal stem cells: potential implications for tumor spreading and wound healing. *Anesthesiology.* 116:841–856. http://dx.doi.org/10.1097/ALN.0b013e31824babfe

Lynes, E.M., and T. Simmen. 2011. Urban planning of the endoplasmic reticulum (ER): how diverse mechanisms segregate the many functions of the ER. *Biochim. Biophys. Acta.* 1813:1893–1905. http://dx.doi.org/10.1016/j.bbamcr.2011.06.011

Lynes, E.M., M. Bui, M.C. Yap, M.D. Benson, B. Schneider, L. Ellgaard, L.G. Berthiaume, and T. Simmen. 2012. Palmitoylated TMX and calnexin target to the mitochondria-associated membrane. *EMBO J.* 31:457–470. http://dx.doi.org/10.1038/emboj.2011.384

Lynes, E.M., A. Raturi, M. Shenkman, C. Ortiz Sandoval, M.C. Yap, J. Wu, A. Janowicz, N. Myhill, M.D. Benson, R.E. Campbell, et al. 2013. Palmitoylation is the switch that assigns calnexin to quality control or ER Ca^{2+} signaling. *J. Cell Sci.* 126:3893–3903. http://dx.doi.org/10.1242/jcs.125856

Matsuo, Y., Y. Nishinaka, S. Suzuki, M. Kojima, S. Kizaka-Kondoh, N. Kondo, A. Son, J. Sakakura-Nishiyama, Y. Yamaguchi, H. Masutani, et al. 2004. TMX, a human transmembrane oxidoreductase of the thioredoxin family: the possible role in disulfide-linked protein folding in the endoplasmic reticulum. *Arch. Biochem. Biophys.* 423:81–87. http://dx.doi.org/10.1016/j.abb.2003.11.003

Matsuo, Y., H. Masutani, A. Son, S. Kizaka-Kondoh, and J. Yodoi. 2009. Physical and functional interaction of transmembrane thioredoxin-related protein with major histocompatibility complex class I heavy chain: redox-based protein quality control and its potential relevance to immune responses. *Mol. Biol. Cell.* 20:4552–4562. http://dx.doi.org/10.1091/mbc.E09-05-0439

Myhill, N., E.M. Lynes, J.A. Nanji, A.D. Blagoveshchenskaya, H. Fei, K. Carmine Simmen, T.J. Cooper, G. Thomas, and T. Simmen. 2008. The subcellular distribution of calnexin is mediated by PACS-2. *Mol. Biol. Cell.* 19:2777–2788. http://dx.doi.org/10.1091/mbc.E07-10-0995

Nymark, P., P.M. Lindholm, M.V. Korpela, L. Lahti, S. Ruosaari, S. Kaski, J. Hollmén, S. Anttila, V.L. Kinnula, and S. Knuutila. 2007. Gene expression profiles in asbestos-exposed epithelial and mesothelial lung cell lines. *BMC Genomics.* 8:62. http://dx.doi.org/10.1186/1471-2164-8-62

Pastorino, J.G., and J.B. Hoek. 2003. Hexokinase II: the integration of energy metabolism and control of apoptosis. *Curr. Med. Chem.* 10:1535–1551. http://dx.doi.org/10.2174/0929867033457269

Patron, M., A. Raffaello, V. Granatiero, A. Tosatto, G. Merli, D. De Stefani, L. Wright, G. Pallafacchina, A. Terrin, C. Mammucari, and R. Rizzuto. 2013. The mitochondrial calcium uniporter (MCU): molecular identity and physiological roles. *J. Biol. Chem.* 288:10750–10758. http://dx.doi.org/10.1074/jbc.R112.420752

Pisoni, G.B., L.W. Ruddock, N. Bulleid, and M. Molinari. 2015. Division of labor among oxidoreductases: TMX1 preferentially acts on transmembrane polypeptides. *Mol. Biol. Cell.* 26:3390–3400. http://dx.doi.org/10.1091/mbc.E15-05-0321

Qi, H., L. Li, and J. Shuai. 2015. Optimal microdomain crosstalk between endoplasmic reticulum and mitochondria for Ca^{2+} oscillations. *Sci. Rep.* 5:7984. http://dx.doi.org/10.1038/srep07984

Raturi, A., and B. Mutus. 2007. Characterization of redox state and reductase activity of protein disulfide isomerase under different redox environments using a sensitive fluorescent assay. *Free Radic. Biol. Med.* 43:62–70. http://dx.doi.org/10.1016/j.freeradbiomed.2007.03.025

Raturi, A., C. Ortiz-Sandoval, and T. Simmen. 2014. Redox dependence of endoplasmic reticulum (ER) Ca^{2+} signaling. *Histol. Histopathol.* 29:543–552.

Redpath, C.J., M. Bou Khalil, G. Drozdzal, M. Radisic, and H.M. McBride. 2013. Mitochondrial hyperfusion during oxidative stress is coupled to a dysregulation in calcium handling within a C2C12 cell model. *PLoS One.* 8:e69165. http://dx.doi.org/10.1371/journal.pone.0069165

Rehman, J., H.J. Zhang, P.T. Toth, Y. Zhang, G. Marsboom, Z. Hong, R. Salgia, A.N. Husain, C. Wietholt, and S.L. Archer. 2012. Inhibition of mitochondrial fission prevents cell cycle progression in lung cancer. *FASEB J.* 26:2175–2186. http://dx.doi.org/10.1096/fj.11-196543

Reitzer, L.J., B.M. Wice, and D. Kennell. 1979. Evidence that glutamine, not sugar, is the major energy source for cultured HeLa cells. *J. Biol. Chem.* 254:2669–2676.

Rizzuto, R., P. Pinton, W. Carrington, F.S. Fay, K.E. Fogarty, L.M. Lifshitz, R.A. Tuft, and T. Pozzan. 1998. Close contacts with the endoplasmic reticulum as determinants of mitochondrial Ca^{2+} responses. *Science.* 280:1763–1766. http://dx.doi.org/10.1126/science.280.5370.1763

Roderick, H.L., J.D. Lechleiter, and P. Camacho. 2000. Cytosolic phosphorylation of calnexin controls intracellular Ca^{2+} oscillations via an interaction with SERCA2b. *J. Cell Biol.* 149:1235–1248. http://dx.doi.org/10.1083/jcb.149.6.1235

Roth, D., E. Lynes, J. Riemer, H.G. Hansen, N. Althaus, T. Simmen, and L. Ellgaard. 2009. A di-arginine motif contributes to the ER localization of the type I transmembrane ER oxidoreductase TMX4. *Biochem. J.* 425:195–205. http://dx.doi.org/10.1042/BJ20091064

Simmen, T., E.M. Lynes, K. Gesson, and G. Thomas. 2010. Oxidative protein folding in the endoplasmic reticulum: tight links to the mitochondria-associated membrane (MAM). *Biochim. Biophys. Acta.* 1798:1465–1473. http://dx.doi.org/10.1016/j.bbamem.2010.04.009

Srere, P.A. 1969. [1] Citrate synthase [EC 4.1.3.7. Citrate oxaloacetate-lyase (CoA-acetylating)]. *Methods Enzymol.* 13:3–11. http://dx.doi.org/10.1016/0076-6879(69)13005-0

Vance, J.E. 1990. Phospholipid synthesis in a membrane fraction associated with mitochondria. *J. Biol. Chem.* 265:7248–7256.

Waldeck-Weiermair, M., A.T. Deak, L.N. Groschner, M.R. Alam, C. Jean-Quartier, R. Malli, and W.F. Graier. 2013. Molecularly distinct routes of mitochondrial Ca^{2+} uptake are activated depending on the activity of the sarco/endoplasmic reticulum Ca^{2+} ATPase (SERCA). *J. Biol. Chem.* 288:15367–15379. http://dx.doi.org/10.1074/jbc.M113.462259

Warburg, O. 1956. On the origin of cancer cells. *Science.* 123:309–314. http://dx.doi.org/10.1126/science.123.3191.309

Ward, P.S., and C.B. Thompson. 2012. Metabolic reprogramming: a cancer hallmark even Warburg did not anticipate. *Cancer Cell.* 21:297–308. http://dx.doi.org/10.1016/j.ccr.2012.02.014

Wu, J., D.L. Prole, Y. Shen, Z. Lin, A. Gnanasekaran, Y. Liu, L. Chen, H. Zhou, S.R. Chen, Y.M. Usachev, et al. 2014. Red fluorescent genetically encoded Ca^{2+} indicators for use in mitochondria and endoplasmic reticulum. *Biochem. J.* 464:13–22. http://dx.doi.org/10.1042/BJ20140931